Improved all-optical OR logic gate based on combined Brillouin gain and loss in an optical fiber

Daisy Williams*, Xiaoyi Bao, and Liang Chen

Department of Physics, University of Ottawa, MacDonald Hall, 150 Louis Pasteur, Ottawa, ON, K1N 6N5, Canada

**Corresponding author: dwill087@uottawa.ca*

Received March 9, 2014; accepted May 20, 2014; posted online July 18, 2014

Improved all-optical OR gates are proposed, using a novel fiber nonlinearity-based technique, based on the principles of combined Brillouin gain and loss in a polarization-maintaining fiber (PMF). Switching contrasts are simulated to be between 82.4%−83.6%, for two respective configurations, and switching time is comparable to the phonon relaxation time in stimulated Brillouin scattering (SBS).

OCIS codes: 200.4660, 060.2310, 190.4370, 190.5890, 200.0200.
doi: 10.3788/COL201412.082001.

Photonic logic has been the focus of many research efforts, and several schemes to improve conventional logic gates have been proposed. Numerous implementations exist, including optically programmable and reversible Boolean logic units[1−3], all-optical logic gates based on integrated optical and waveguide structure Mach-Zehnder interferometers (MZIs)[4−6], the use of nonlinear optical processes in semiconductor optical amplifiers (SOAs)[7−10], and the use of a combination thereof: integrated MZIs based on SOA[11−16]. Additionally, there are logic gates proposed by terahertz optical asymmetric demultiplexer (TOAD) based switches[17−20]. Techniques based on the design of simple passive optical components also exist. These include optical logic parallel processors[21], as well as the multi-output polarization-encoded optical shadow-casting scheme[22]. In fiber nonlinearity-based techniques, the Kerr effect is used in highly nonlinear fibers (HNLFs) to induce birefringence-thereby rotating the polarization state of an output light wave[23,24] and using it as a switching mechanism.

A novel combined Brillouin gain and loss process in a polarization-maintaining fiber (PMF) was proposed to realize all-optical NAND/NOT/AND/OR logic gates in the frequency domain[25]. The combination of simultaneous gain and loss improves the signal-to-noise ratio (SNR) by approximately twofold[26]. Additionally, the PMF ensures the technique to be free of polarization induced signal fluctuations or polarization mode dispersion (PMD), which is caused by birefringence-induced error in conventional fiber nonlinearity-based techniques.

In this letter, we propose new and improved configurations of all-optical OR logic gates. We propose configurations comprising a combination of NAND and NOT gates, which have the advantage of having a much simpler switching system, while maintaining the same switching contrasts as the OR gate configuration in Ref. [25].

The process of stimulated Brillouin scattering (SBS) has been studied in a single mode optical fiber, with core radius of 4.1 μm. The configuration is comprised of a continuous wave (CW) launched into one end, and a Stokes wave (SW) and an anti-Stokes wave (ASW) launched into the other end. The schematic arrangement is shown on Fig. 1.

The system operates in the steady-state regime with pulse lengths greater than the phonon relaxation time, in this case 10 ns[27,28]. In the slowly varying amplitude approximation, the interaction between the CW, SW, ASW, and two acoustic waves (AW_1 and AW_2), as shown in Fig. 1, is described by the following system of equations[25,29].

$$-\frac{dA_1}{dz} = \frac{i\omega_1\gamma_e}{2nc\rho_0}\rho_1 A_2 + \frac{i\omega_1\gamma_e}{2nc\rho_0}\rho_2^* A_3 - \frac{1}{2}\alpha A_1, \quad (1)$$

$$\frac{dA_2}{dz} = \frac{i\omega_2\gamma_e}{2nc\rho_0}\rho_1^* A_1 - \frac{1}{2}\alpha A_2, \quad (2)$$

$$\frac{dA_3}{dz} = \frac{i\omega_3\gamma_e}{2nc\rho_0}\rho_2 A_1 - \frac{1}{2}\alpha A_3, \quad (3)$$

$$(\Omega_B^2 - \Omega_1^2 - i\Omega_1\Gamma_B)\rho_1 = \frac{\gamma_e q_1^2}{4\pi} A_1 A_2^*, \quad (4)$$

$$(\Omega_B^2 - \Omega_2^2 - i\Omega_2\Gamma_B)\rho_2 = \frac{\gamma_e q_2^2}{4\pi} A_3 A_1^*, \quad (5)$$

where $\Omega_1 = \omega_1 - \omega_2$, $\Omega_2 = \omega_3 - \omega_1$. The angular frequencies and complex amplitudes of the AW_1 and AW_2 are denoted as Ω_1 and ρ_1, and Ω_2 and ρ_2, respectively; A_1, A_2, and A_3 are the complex amplitudes of the CW, SW, and ASW, respectively; c is the speed of light; ρ_0 is the density of the fiber; γ_e is the electrostrictive constant; z is the coordinate along the fiber; n is the index of refraction of the fiber; v is the speed of sound in the fiber; Γ_B is the Brillouin line width; Ω_B is the Brillouin frequency defined as $\Omega_B = 2nv\omega_1/c$, where ω_1, ω_2, and ω_3 are the angular frequencies of the CW, SW, and ASW, respectively.

The system of Eqs. (1)−(5) was solved numerically[25], making use of the following parameters of the fiber: n=1.48, γ_e=0.902, λ=1550 nm, ρ_0 =2.21 g/cm^3, v=5616 m/s, Γ_B=0.1 GHz, α=0.2 dB/km, and the power penalty is 0.67 dB/km. P_{10}, P_{20}, and P_{30} are the input powers of the CW, SW, and ASW, respectively, while $P_{1-\mathrm{out}}$ and $P_{3-\mathrm{out}}$ are the output powers of the CW and the ASW.

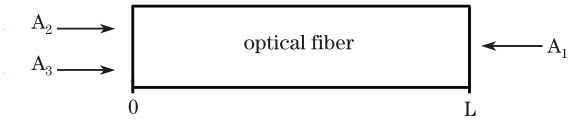

Fig. 1. Schematic arrangement of SBS in a PMF of length L. A_1: CW, A_2: SW, and A_3: ASW.

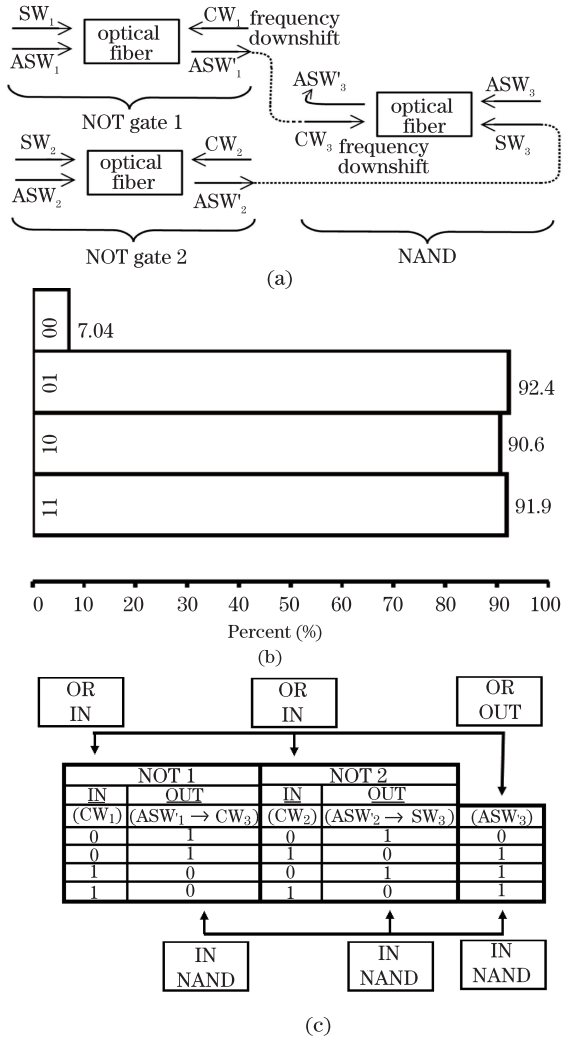

Fig. 2. (a) Schematic of configuration X: OR gate, (b) OR gate switching contrast plot, and (c) OR gate logic table. Low threshold: 7.04%, high threshold: 90.6%, and tolerance: 83.6%.

The NAND and NOT gates of this letter have been characterized by their truth tables, where '0' and '1' are logical values of the truth table. For the current study, a power of 0.1 mW was assigned to have a logical value of '0', while a power of 10 mW was assigned to have a logical value of '1'.

In the NAND gate configuration in Ref. [25], P_{10} and P_{20} are used as input signals, P_{30} is used as the reference signal, and the output ASW power, $P_{3-\mathrm{out}}$, is used as the output signal of the NAND gate. This configuration requires a tunable laser source, capable of detuning the SW and ASW separately by up to $\pm 3\Gamma_B$. In this configuration, the reference ASW signal was held constant at P_{30}=10 mW.

In the 3-wave NOT gate configuration in Ref. [25], P_{10} was chosen to be the input signal, and the output ASW power, $P_{3-\mathrm{out}}$, was taken to be the output signal of the optical gate. In this case, the reference SW and ASW signals were held constant at $P_{20} = P_{30}$=10 mW. Similarly, in the 2-wave NOT gate configuration, which only had a CW and a SW, P_{20} was chosen to be the input signal, and the output CW power, $P_{1-\mathrm{out}}$, was chosen to be the output signal of the optical gate. The input CW signal was taken to be the reference signal, and was held constant at P_{10}=10 mW.

Because of the narrowband characteristic of the Brillouin amplification, the bit rate of the signal is limited to tens of megabits per second[30,31]. However, there are a number of techniques aimed at increasing the Brillouin gain bandwidth, thereby supporting a higher bit rate. These include a simple pump-spectral broadening technique[32,33] via direct- modulation of the pump laser using a pseudorandom binary sequence (PRBS) data, a Gaussian noise source. Alternatively, the pump wave can be broadened by using an external phase modulator (PM), which has been demonstrated to yield bit rates between 1 and 2.5 Gb/s[30,34]. Comparatively, bit rates between 10 and 100 Gb/s have been claimed by other technologies to construct optical logic units[6,12,15,16,18,20]. Though these alternative constructions have higher bit rates, they also include numerous drawbacks, including configurations which are both bulky and require extensive calibration, and fall victim to spontaneous emission noise, time dependent modulation due to time jitter, and birefringence induced signal distortion. The technique based on combined Brillouin gain and loss, disclosed in this letter, is free of polarization-induced signal fluctuations which cause spectral distortion, thereby making the lower bit rate a worthy trade-off.

In configuration X, an OR gate is constructed by connecting a NAND gate with two 3-wave NOT gates, shown schematically in Fig. 2.

CW_1, as well as CW_2, in Fig. 2(a) and (c), are the input signals of NOT gate 1 and NOT gate 2, respectively, as well as the two input signals of the OR gate. Similarly, SW_1 and ASW_1, as well as SW_2 and ASW_2, are the reference signals of each NOT gate, which are held constant at 10 mW. The output ASW'$_1$ signal from NOT gate 1 is frequency downshifted from ω_3 to ω_1, turning it into an effective CW_3 wave, which is an input signal for the NAND gate. The output ASW'$_2$ signal from NOT gate 2 is frequency downshifted, from ω_3 to ω_2, turning it into an effective SW_3 wave, which is another input signal for the NAND gate. The reference signal of the NAND gate, ASW_3, is held constant at 10 mW. The output signal of the OR gate is the ASW'$_3$ signal. Output powers of 0.704, 9.24, 9.06, and 9.19 mW were obtained for the logical inputs '0 0', '0 1', '1 0', and '1 1', respectively. A fiber length of L=350 m was used for all three gates.

As can be seen from Fig. 2(b), configuration X of the OR gate yields a high switching contrast of 83.6%. This is comparable to the OR gate proposed in Ref. [25], which has a switching contrast of 83.0%. Additionally, NOT gate 1 and NOT gate 2 have only one input each, namely CW_1 and CW_2 respectively. The SW_1 and ASW_1, and SW_2 and ASW_2, respectively, are kept as reference signals. In the OR gate of configuration IX, proposed in Ref. [25], a NAND gate 1 and a NAND gate 2 are employed each having two input signals, CW_1 and SW_1, and CW_2 and SW_2, respectively, which must be carefully calibrated to match each other for each logical input. Such calibration is time-consuming, and often difficult to achieve. Configuration X eliminates this difficulty by employing NOT gate 1 and NOT gate 2, which by virtue of the operation of a NOT gate, have only one

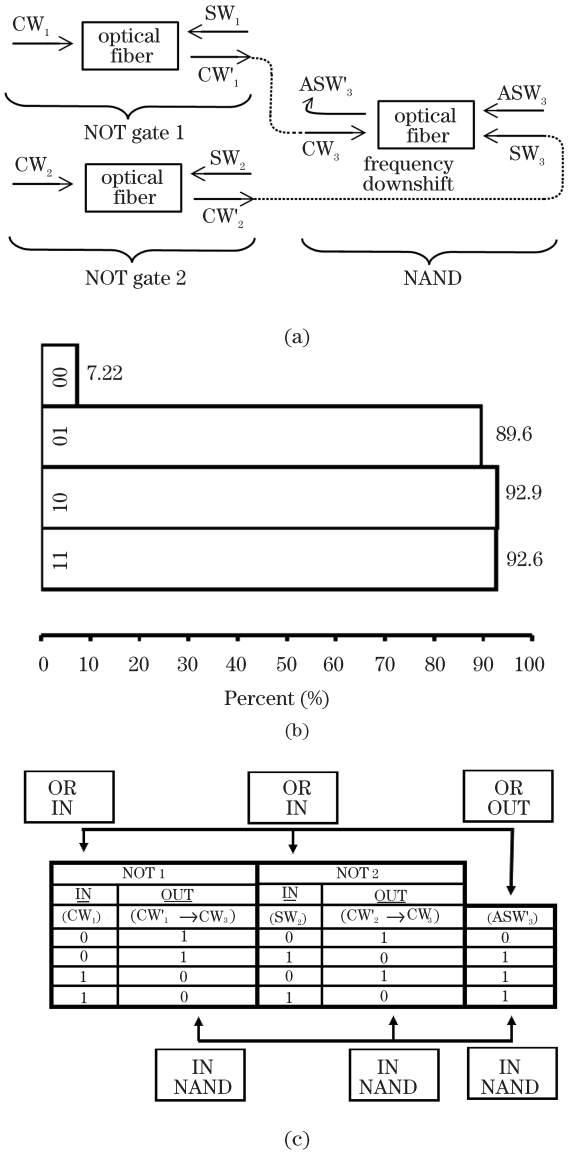

Fig. 3. (a) Schematic of configuration XI: OR gate, (b) OR gate switching contrast plot, and (c) OR gate logic table. Low threshold: 7.22%, high threshold: 89.6%, and tolerance: 82.4%.

input signal each, and do not require any such calibration. As a result, configuration X of the all-optical OR gate has the benefit of being simpler to operate and more compact as compared to existing variants[25].

In configuration XI, an OR gate is constructed by connecting a NAND gate with two 2-wave NOT gates, shown schematically in Fig. 3.

SW_1, as well as SW_2, in Figs. 3(a) and (c), are the input signals of NOT gate 1 and NOT gate 2, respectively, as well as the two input signals of the OR gate. Similarly, CW_1 and CW_2 are the reference signals of NOT gate 1 and NOT gate 2, respectively, which are held constant at 10 mW. The output CW'$_1$ signal from NOT gate 1 is redirected towards the NAND gate into an effective CW_3 wave, which is an input signal for the NAND gate. The output CW'$_2$ signal from NOT gate 2 is frequency downshifted from ω_1 to ω_2, turning it into an effective SW_3 wave, which is another input signal for the NAND gate. The reference signal of the NAND gate, ASW_3, is held constant at 10 mW. The output signal of the OR gate is the ASW'$_3$ signal. Output powers of 0.722, 8.96, 9.29, and 9.26 mW were obtained for the logical inputs '0 0', '0 1', '1 0', and '1 1', respectively. A fiber length of L=350 m was used for all three gates.

As can be seen from Fig. 3(b), configuration XI of the OR gate yields a high switching contrast of 82.4%. In addition to the existing benefits of using two NOT gates in place of two NAND gates, as discussed previously, another benefit of configuration XI is that only one frequency downshift is required, from CW'$_2$ to SW_3, which greatly increases the accuracy and ease of operation, while decreasing the bulk. In summary, the setup of configuration XI is even simpler to operate and more compact than that of configuration X, without any significant compromise on switching contrast.

In conclusion, two new and improved configurations for an all-optical OR gate are proposed, based on the principles of combined Brillouin gain and loss in a PMF. Switching contrasts are simulated to be between 82.4%−83.6%, for the two respective configurations. The configurations X and XI are advantageous in comparison to the OR gate in Ref. [25], since they have a comparable switching contrast, yet are simpler in implementation and operation, and are more compact due to the added simplicity of having two NOT gates in place of two NAND gates. Configuration XI is even more beneficial, since only one frequency downshift is needed, thereby improving it's operation and compactness. For this reason, the configurations proposed in this letter have the potential to greatly improve the construction of all-optical signal processing units.

The authors would like to acknowledge the financial support of NSERC Discovery Grants and the Canada Research Chair (CRC) Program.

References

1. T. Chattopadhyay, Appl. Opt. **52,** 6049 (2011).
2. T. Chattopadhyay, Appl. Opt. **51,** 5266 (2012).
3. M. R. Fetterman, IEEE Photon. Technol. Lett. **21,** 1740 (2009).
4. Y. Wu, T. Shih, and M. Chen, Opt. Express **16,** 248 (2008).
5. M. Nazari and M. Haghparast, Aust. J. Basic App. Sci. **5,** 923 (2011).
6. T. Chattopadhyay, IEEE J. Sel. Topics Quantum Electron. **18,** 585 (2012).
7. Z. Li and G. Li, Photon. Technol. Lett. **18,** 1341 (2006).
8. S. H. Kim, J. H. Kim, B. G. Yu, Y. T. Byun, Y. M. Jeon, S. Lee, D. H. Woo, and S. H. Kim, Electron. Lett. **41,** 1027 (2005).
9. D. Nesset, T. Kelly, and D. Marcenac, IEEE Commun. Mag. **36,** 56 (1998).
10. C. Schubert, R. Ludwig, and H-G. Weber, J. Opt. Fiber Common. Reports **2,** 171 (2004).
11. X. Ye, P. Ye, and M. Zhang, Opt. Fiber. Tech. **12,** 312 (2006).
12. T. Chattopadhyay, IET Optoelectron. **5,** 270 (2011).
13. K. I. Kang, T. G. Chang, I. Glesk, and P. R. Prucnal, Appl. Opt. **35,** 417 (1996).
14. J. Y. Kim, J. M. Kang, T. Y. Kim, and S. K. Han, J. Lightwave Technol. **24,** 3392 (2006).

15. L. Yi, W. Hu, H. He, Y. Dong, Y. Jin, and W. Sun, Chin. Opt. Lett. **9,** 030603 (2011).
16. J. Yang, L. Han, H. Zhang, and Y. Guo, Chin. Opt. Lett. **5,** 566 (2007).
17. Z. Y. Shen and L. L.Wu, Appl. Opt. **47,** 3737 (2008).
18. T. Chattopadhyay, Optik **122,** 1486 (2011).
19. T. Chattopadhyay, J. Nonlinear Opt. Phys. Mater. **18,** 471 (2009).
20. T. Chattopadhyay, Opt. Fiber Tech. **17,** 558 (2011).
21. A. W. Lohmann, Appl. Opt. **25,** 1594 (1986).
22. M. A. Karim, A. A. S. Awwal, and A. K. Cherri, Appl. Opt. **26,** 2720 (1987).
23. C. Yu, L. Christen, T. Luo, Y. Wang, Z. Pan, L. Yan, and A. E. Willner, Photon. Technol. Lett. **17,** 1232 (2005).
24. C. Yu, L. Christen, T. Luo, Y. Wang, Z. Pan, L. Yan, and A. E. Willner, in *Proceedings of CLEO 2004* 3 (2004).
25. D. Williams, X. Bao, and L. Chen, Appl. Opt. **52,** 3404 (2013).
26. W. Zou, C. Jin, and J. Chen, Appl. Phys. Express **5,** 082503 (2012).
27. R. Boyd, *Nonlinear Optics* (Academic Press, 1992).
28. D. Williams, X. Bao, and L. Chen, Photon. Res. **2,** 1 (2014).
29. X. Bao and L. Chen, Sensors **11,** 4152 (2011).
30. L. Yi, L. Zhan, W. Hu, and Y. Xia, IEEE Photon. Technol. Lett. **19,** 619 (2007).
31. M. Lee, R. Pant, and M. A. Neifeld, Appl. Opt. **47,** 6404 (2008).
32. M. G. Herraez, K. Y. Song, and L. Thevenaz, Opt. Express **14,** 39 (2006).
33. Z. Zhu, A. M. C. Dawes, D. J. Gauthier, L. Zhang, and A. E. Willner, in *Proceedings of OFC2006* PDP1 (2006).
34. L. Yi, L. Zhan, Y. Su, W. Hu, L. Leng, Y. Song, H. Shen, and Y. Xia, in *Proceedings of ECOC 2006* We3.P.30 (2006).